

Theory of chiral periodic mesophases formed from an achiral liquid of bent-core molecules

V. L. Lorman¹ and B. Mettout²¹*LPMT, CNRS-Université Montpellier II, place Eugène Bataillon, 34095 Montpellier, France*²*LPTM, 33 rue St Leu, 80000 Amiens, France*

(Received 17 October 2003; revised manuscript received 23 January 2004; published 9 June 2004)

The theory of unconventional one-dimensional periodic mesophases forming in a liquid of achiral bent-core molecules is presented. The order parameter is a polarization wave. Three distinct phases which can be stabilized directly from the isotropic liquid phase are associated with linear, circular, and elliptic polarizations of the wave. The elliptic polarization leads to the structure of the commonly studied B_2 "bent-core" mesophase whereas the recently discovered C_p phase may be assigned to the linear polarization. We present the molecular configurations and macroscopic properties of the stable states. Their behavior under chiral doping and electric field application are investigated and the corresponding phase diagrams are calculated.

DOI: 10.1103/PhysRevE.69.061710

PACS number(s): 61.30.Cz, 64.70.Md.

I. INTRODUCTION

The discovery in 1996 of ferroelectric switching in "bent-core" mesophases by Niori *et al.* [1], followed by the demonstration of their antiferroelectric character [2], opened up a new way in the liquid crystal science. Although at first view these systems fit into the sequence of well-known ferroelectric and antiferroelectric smectic (Sm) phases [3], a number of striking peculiarities prevents the confusion between usual calamitic and bent-core antiferroelectric phases. First of all, in calamitics the local polarization results from the chiral character of rodlike molecules while bent-core mesophases are made with achiral molecules. Their symmetry group C_{2v} [4] permits a strong electric dipolar moment and an intrinsic optical biaxiality which lead to peculiar physical behaviors (especially electro-optic) and potential technological applications.

At least eight phases, denoted B_1 to B_8 , have yet been disclosed in bent-core compounds. None of them has been found in pure calamitic systems. The most commonly studied B_2 phase, which appears below the isotropic liquid, has a smectic antiferroelectric chiral structure [2,5]. Numerous two- and three-dimensional structures have also been evidenced. The B_5 phase presents short-range translational order [6], associated with a rectangular molecular arrangement. Similar two-dimensional (2D) lattices are also claimed for the B_1 and B_6 phases [7,8]. In phase B_7 , x-ray experiments and observations of unusual textures lead to assume a helical structure [9] with 2D long-wavelength modulations [10]. Finally, the B_3 [5,7,11] and B_4 [7,11] phases present 3D translational order [12].

Within this rich polymorphism, the smectic-A and nematic phases are quite rare. This absence of intermediate phases between the isotropic liquid and the antiferroelectric states is surely the most significant difference with respect to calamitic systems. In calamitics the orientational and translational ordering of the molecules are independent degrees of freedom which condense at different temperatures, leading to the classical sequence on cooling: isotropic \rightarrow nematic \rightarrow Sm-A \rightarrow Sm-C... Independent order parameters account for each step in this sequence: The nematic tensor breaks the isotropic symmetry of the liquid state, the smectic density wave

breaks the translational symmetry of the nematic phase and the tilt axial-vector order parameter breaks the 2D isotropic symmetry of the smectic layers in the Sm-C phase. In the bent-core mesophases, all these orders appear simultaneously and form directly antiferroelectric smectic phases from the isotropic liquid. By assuming combination of classical mechanisms, this complex process is only possible across a strongly first-order transition when the liquid state becomes simultaneously unstable with respect to all the previously mentioned primary order parameters. Nevertheless it is very unlikely that, on the one hand, several order parameters condense simultaneously, while on the other hand, almost no phase corresponding to a single order parameter (nematic or smectic) is reported in the examined molecular series.

These properties are reminiscent of the situation known for a few decades in superconductors [13]. In the unconventional superconducting or superfluid systems, namely, the heavy-fermions crystals [14], the organic and high- T_C superconductors [15] or the superfluid phases of He₃ [16], the low-temperature phases exhibit simultaneously superconducting, magnetic, and structural modifications. Each one is associated with the breakdown of a specific part of the parent phase symmetry group: gauge, rotational, and time reversal operations, respectively. Furthermore, no phase is observed in which a single symmetry is broken and the transitions toward the ordered phases are often second order. It was long recognized that this complex process cannot be accounted for by the simultaneous onset of classical order parameters. Instead, a single order parameter, associated with p - or d -anisotropic wave functions [17], gathers in a single representation all the relevant degrees of freedom involved in the transition. Thus it explains in a very simple way the complex properties of the ordered phases along with the simple thermodynamic behavior observed at the corresponding transitions.

Along the same lines, we have proposed [18] a model based upon a single order parameter accounting for the translational, rotational, and chiral symmetry breakdowns evidenced in bent-core systems. This model is dual with the d -wave theory of lamellar high- T_C oxide superconductors [19]. The purpose of this article is to present the main physical consequences of this model and to briefly compare them

with the available experimental data. The order parameter is a transverse polarization wave condensing in the isotropic liquid. On the one hand, the wave aspect of the order parameter breaks the continuous translational symmetry of the liquid along the direction of the wave vector [20]. On the other hand, the polar vector aspect leads to the rotational symmetry breakdown within the smectic layers. This model predicts three stable phases in which the vector wave is circularly, linearly, or elliptically polarized. In the nonsmectic “circular” phase a regular chiral helix is formed on the molecular scale. In the “linear” phase the polarization is confined within a single plane and the structure is smectic but remains achiral. The “elliptic” structure is chiral, antiferroelectric, and smectic.

The comparison of the model predictions with the x-ray, dielectric, and electro-optic data shows that the elliptic phase corresponds to the homochiral state observed in the B_2 phase whereas the linear phase may be assigned to the recently discovered antiferroelectric C_p phase [21] (denoted $\text{Sm}AP_A$ in Ref. [22]). We propose that the circular structure could possibly describe the yet unknown structure of the B_7 phase in the vicinity of the isotropic liquid.

The paper is organized as follows. In Sec. II we present the ordered phases and the theoretical phase diagrams. In Sec. III the static macroscopic properties in each phase are worked out. Section IV is devoted to the effects of chiral doping and electric field application. In Sec. V, a brief comparison with previous theories and the available experimental data is given.

II. ORDERED PHASES

Most of the dipolar ordered (ferroelectric, antiferroelectric, or ferrielectric) phases in chiral calamitic liquid crystals result from a phase transition from the paraelectric smectic-A (Sm-A) parent structure [23]. On the contrary, in the media of achiral bent-core molecules, one observes that the antiferroelectric phase is almost always formed directly from the isotropic liquid [4]. This suggests a new transition mechanism in which a single instability of the isotropic state is involved, instead of the double instability describing the polar ordering in chiral systems. Within this hypothesis of a single transition mechanism, experimental data provide an unambiguous choice of the order parameter as a transverse vector wave. Indeed the most common low-symmetry state in this system, denoted B_2 is characterized by one-dimensional periodicity, local polarization perpendicular to the periodicity direction, and zero macroscopic polarization [2,4].

A. The vector-wave mechanism

The polar-vector wave associated with a single wave vector \mathbf{k} leads to a one-dimensional structure with wavelength $\lambda=2\pi/k$. Let z be the direction of \mathbf{k} . The general form of a transverse vector wave can be written as

$$\vec{P}(z) = \vec{e}_x [p_x \cos(kz + \varphi_x)] + \vec{e}_y [p_y \cos(kz + \varphi_y)], \quad (1)$$

where p_x and p_y are the components of the wave amplitude, φ_x and φ_y are the initial phases, and \mathbf{e}_x and \mathbf{e}_y are unit vectors

in the plane normal to \mathbf{k} . The polar vector $\mathbf{P}(z)$ represents the local polarization. Equation (1) describes a helical structure with elliptical shape which depends on four parameters (p_x , p_y , φ_x , and φ_y) defining its shape, position in space, and orientation. By varying these parameters one can obtain specific structures with various symmetry groups. For a more convenient symmetry analysis of the model let us make the following change of variables in Eq. (1):

$$\eta_1 = p_x e^{i\varphi_x} - i p_y e^{i\varphi_y}, \quad \eta_2 = p_x e^{-i\varphi_x} - i p_y e^{-i\varphi_y}, \quad (2)$$

$\eta_1 = \rho_1 e^{i\varphi_1}$, $\eta_2 = \rho_2 e^{i\varphi_2}$, η_1^* and η_2^* are the complex amplitudes of $\mathbf{P}(z)$. The angles φ_1 and φ_2 are Goldstone variables responsible on the orientation and the position of the structure in space. The moduli ρ_1 and ρ_2 are energetic variables which define the ellipse shape, $2(\rho_1 + \rho_2)$ and $2|\rho_1 - \rho_2|$ being the big and the small axes of the ellipse, respectively.

The wave (2) spans an irreducible representation of the symmetry group $G_L = O(3) \times T_3$ of the parent achiral liquid. It is associated with a formally infinite-dimensional space (corresponding to waves directed in any direction of space), but the considered 1D periodic antiferroelectric structures can be described by an effective order parameter which has only four components η_1 , η_2 , η_1^* , and η_2^* . According to Landau theory [24], the free energy F is invariant with respect to the subgroup G_{eff} of G_L which preserves the direction of the single wave vector \mathbf{k} [25,26]. It can be easily seen that $G_{\text{eff}} = D_{\infty h} \times T_3$ contains the inversion I , the continuous rotations C_ϕ about z , the twofold rotations U_2 normal to \mathbf{k} , the mirror planes σ parallel or normal to \mathbf{k} and the 3D continuous translations T_r .

B. Ordered phases

The integrity basis [27] of the vector-wave representation consists of two independent invariants

$$I_1 = \rho_1^2 + \rho_2^2, \quad I_2 = \rho_1^2 \rho_2^2. \quad (3)$$

The general form of the homogeneous part of the free energy then reads

$$F_P = a_{10} I_1 + a_{01} I_2 + a_{11} I_1 I_2 + \dots + a_{np} I_1^n I_2^p + \dots, \quad (4)$$

where a_{np} is a phenomenological coefficient. Minimization of F_P with respect to the effective order-parameter components provides four stable states.

(I) The isotropic liquid phase denoted L when $\rho_1 = \rho_2 = 0$.

(II) For $\rho_1 \neq 0$, $\rho_2 = 0$ (or equivalently $\rho_1 = 0$, $\rho_2 \neq 0$) a chiral helielectric phase, denoted “circular” (C phase), is stabilized. It has the structure of a circularly polarized wave. Since in C $p_x = p_y$ and $\varphi_x - \varphi_y = m\pi/2$ (m integer), the vector wave becomes

$$\vec{P}(z) = p_x \vec{e}_x \cos(kz + \varphi_x) - p_y \vec{e}_y \sin(kz + \varphi_x). \quad (5)$$

(III) For $\rho_1^2 = \rho_2^2$ an achiral antiferroelectric phase, denoted “rectilinear” (R -phase), is stabilized. It has the structure of a linearly polarized wave. The wave parameters are related by $\varphi_x - \varphi_y = m\pi$ (m integer). In this phase, the polarization field takes the form

$$\vec{P}(z) = [p_x \vec{e}_x + p_y \vec{e}_y] \cos(kz + \varphi_x). \quad (6)$$

(IV) The intermediate phase, denoted “elliptic” (EL phase), characterized by $\rho_1 \neq \rho_2$, corresponds to the general transverse wave with elliptic polarization [see Eq. (2)].

Let us now discuss the properties of these structures.

C phase. The symmetry group $G_C = \infty_1 22$ (in Shubnikov’s-type notation [28] for a nonsymmorphic space group) of the circular phase belongs to the D_∞ uniaxial symmetry class. It is periodic along z and remains homogeneous in the x - y plane. Although the continuous translations T_z , as well as the continuous rotations C_θ are broken, all the helical combinations $T_{-\theta/k} C_\theta$ are preserved and forbid a smectic modulation of the density. Note that the local point group C_2 permits a nonzero local transverse polarization $\mathbf{P}(z)$ but the global helical symmetry cancels the macroscopic polarization. The most striking property of this structure is the spontaneous breaking of spatial inversion in an achiral medium which makes it chiral. Two types of energetically equivalent domains with opposite signs of the chirality should result from this symmetry breakdown. In two different domains the helices are wound in opposite senses.

R phase. The symmetry group $G_R = Pmma$ of the rectangular phase belongs to the D_{2h} achiral biaxial symmetry class. At general position the local symmetry is C_S whereas it becomes C_{2v} at positions where \mathbf{P} is maximum and C_{2h} where \mathbf{P} vanishes. The local transverse polarization $\mathbf{P}(z)$ remains within a single plane containing the z axis but its amplitude varies with z . The macroscopic polarization vanishes yielding a planar antiferroelectric structure. The discrete periodicity of the R phase is associated with the onset of a smectic density wave. It might be compared (but not identified) with the unwound chiral Sm- C_A antiferroelectric phase though the R phase remains achiral and with the anticlinic Sm- O phase [29] found in achiral calamitic liquid crystals.

EL phase. The symmetry group $G_{EL} = P222_1$ of the elliptic phase belongs to the D_2 biaxial symmetry class. Its has the same translational symmetry and smectic feature as the R phase. The transverse twofold axes are located at the maximums and minimums of $\mathbf{P}(z)$ and are parallel to the principal axes of the projected ellipse. The macroscopic polarization still vanishes but the corresponding antiferroelectric structure is not planar and is chiral.

C. Molecular configurations

The simplest way to describe the molecular order consists in assuming that, at a given position z in the structure, all the molecules are oriented along the same direction. The orientation of one molecule at a given position z is determined by the local point group denoted $G_p(z)$. This procedure is similar to the determination of the so-called “motifs” in classical crystallography. In the E , R , and EL phases there are only five nonequivalent positions with local point groups: C_{2v} , C_{2h} , C_2 , C_s , or C_1 . $G_p(z) = C_2$, everywhere in the circular phase. In the EL phase the general and special positions have C_1 and C_2 symmetry, respectively. In the R phase $G_p(z)$ can be C_S , C_{2v} or C_{2h} (where \mathbf{P} vanishes). The situation $G_p(z) = C_{2h}$ is specific because C_{2h} is not a subgroup of the mo-

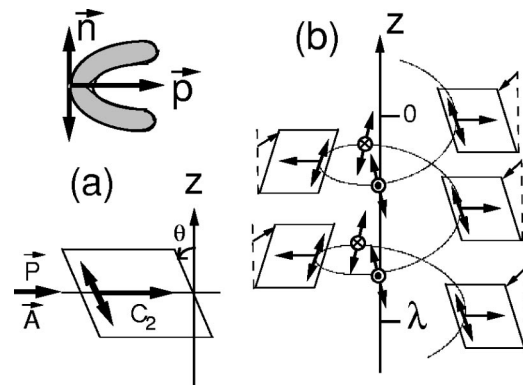


FIG. 1. Molecular configuration in the C phase. (a) Molecular orientation at one position in the C phase. (b) Molecular configuration in one unit cell of the C phase. At $z=0$ the molecule is oriented as in (a). At other positions the previous configuration precesses about the z axis. All the molecules belonging to a single plane normal to Oz are oriented in the same way. The helix drawn in the figure is a help for visualizing the precession of the molecular orientation but it has no direct physical meaning.

lecular symmetry group C_{2v} . The fact that at this positions \mathbf{P} vanishes indicates that some statistical disorder must be introduced in the molecular orientation: the molecules which have their center localized where $\mathbf{P}=0$ have equal probabilities to have their polarization \mathbf{p} oriented along $+Ox$ or along $-Ox$. Slightly above and below this position, the corresponding “up-down” disorder decreases and becomes minimal where \mathbf{P} is maximum.

In the C phase, presented in Fig. 1, the orientation of the molecular polarization \mathbf{p} precesses periodically around the z axis. The molecular plane is tilted to a constant angle around \mathbf{p} with respect to the local \mathbf{p} - Oz plane.

In the R phase $G_p(z)$ varies from C_S at general position to C_{2h} where $\mathbf{P}=0$ or C_{2v} where \mathbf{P} is maximum. At the latter position \mathbf{p} is oriented along the C_2 axis and the molecular plane is parallel to Oz . At general position z , the molecular plane is rotated to an angle $\phi(z)$ with respect to the previous configuration. $\phi(z)$ is a periodic function of z vanishing at positions with C_{2v} symmetry and maximum at positions with C_{2h} symmetry. At low temperature the amplitude of the induced density modulation becomes so strong that almost all the molecules are gathered about the planes of maximum density (center of the smectic layers). The symmetry of the R phase permits only two positions for the density maximums.

(i) Where \mathbf{P} is maximum. The corresponding state is a two-layer stacking of molecules with polarization perpendicular to Oz . The direction of the polarization is opposite in two adjacent layers. Moreover, the molecular plane is not tilted and the flip disorder is minimal. This yields the antiferroelectric structure depicted in Fig. 2(a).

(ii) At the zeroes of \mathbf{P} . The corresponding structure is a two-layer stacking of nonpolar tilted subunits with alternating orientations. This yields an anticlinic structure represented in Fig. 2(b). Let us notice that, though \mathbf{P} vanishes at the maximum of the density, a residual antiferroelectricity can never be completely neglected due to the polarization of molecules slightly above or below the smectic planes and to

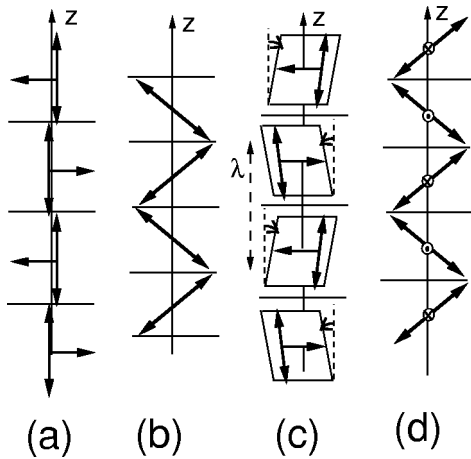


FIG. 2. Limit structures of the R and EL phases arising when the induced density wave is sufficient to single out the molecular configurations located at density maximums. The density minimums are indicated by straight horizontal lines. (a) R phase when the maximums of density coincide with the polarization maximums. The structure is mainly antiferroelectric. (b) R phase when the density maximums coincide with the zeroes of the polarization wave. The structure is mainly antclinic. (c) EL phase resulting from the deformation of the R phase depicted in (a). (d) EL -phase resulting from deformation of (b). In this picture of the EL phase the polarization wave seems linearly polarized because the molecular orientations between the density maximums are omitted.

the delocalization of the polarization density within a single molecule.

Which case is more stable depends on the sign of the coupling between the density wave and the order parameter [see Eq. (13)]. When the $L \rightarrow R$ transition is second order the sign of the coupling coefficient is fixed and only one case can be realized, either antiferroelectric or antclinic. For a strongly first-order $L \rightarrow R$ transition the sign of the coupling can change. As it becomes negative, the system can undergo a smooth transformation from the antiferroelectric to the antclinic state without any phase transition.

The description of the elliptic phase at low temperature is similar. Close to the R phase, two limit cases can also be defined. (i) In the first one [Fig. 2(c)] the maximums of the density coincide with those of \mathbf{P} . The molecular plane is slightly tilted in opposite directions in two adjacent layers. (ii) In the second one [Fig. 2(d)] the maximums of the density coincide with the maximums of the tilt angle but with nonzero value of \mathbf{P} . These two configurations can be clearly distinguished only in the vicinity of R . At lower temperature they become qualitatively equivalent. Indeed when neither the mean polarization nor the tilt are negligible, Fig. 2(d) may be viewed as resulting from Fig. 2(c) after a rotation to 90° together with a translation of a quarter of the period λ .

D. Phase diagrams and modulated structures

Equations (4) and (5) permit us to calculate typical phase diagrams predicted by the vector-wave model. The most simple phase diagram presenting stability regions for all four

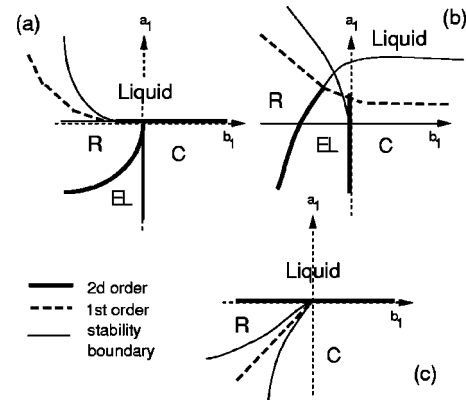


FIG. 3. Theoretical phase diagrams of the homogeneous vector-wave model. (a) For the free energy given by Eq. (7a). (b) For the free energy (7b). (c) For the free energy (7c).

phases can be calculated by using the following truncated free energy [30]:

$$F_P = a_1(\rho_1^2 + \rho_2^2) + b_1 \rho_1^2 \rho_2^2 + \frac{a_2}{2}(\rho_1^2 + \rho_2^2)^2 + \frac{b_2}{2} \rho_1^4 \rho_2^4 \quad (7a)$$

with $a_1 = a_0(T - T_C)$, $a_2, b_2 > 0$. In the corresponding phase diagram, presented in Fig. 3(a), the isotropic liquid is separated from the C phase by a line of second-order phase transformation. The transition between the L and R phases changes its order from second to first at a tricritical point. The stability region of the elliptic phase is limited by lines of second-order phase transitions toward the phases C and R . All the phases merge at a Landau point O [27]. Within a model corresponding to a higher degree of nonlinearity, the free energy can be written

$$F_P = a_1 I_1 + b_1 I_2 + \frac{a_2}{2} I_1^2 + \frac{b_2}{2} I_2^2 + \frac{a_3}{3} I_1^3 \quad (7b)$$

with $a_2 < 0$, $b_2 > 0$, $a_3 > 0$. Accordingly, the previous phase diagram is modified in the following respects [see Fig. 3(b)]: Two three-phase points (T_1 and T_2) replace the Landau point. The transitions from the liquid to the phases C and R are now strictly firstorder. In addition, a direct first-order transition between the liquid and the elliptic state EL becomes possible. The transitions between antiferroelectric phases remain second order.

In a third typical model, the free energy, given by

$$F_P = a_1 I_1 + b_1 I_2 + \frac{a_2}{2} I_1^2 + \frac{b_2}{2} I_2^2 + c I_1 I_2. \quad (7c)$$

($a_2, b_2 > 0$, $a_2 b_2 - c^2 < 0$), leads to the phase diagram shown in Fig. 3(c). Its main feature, the absence of stability region for the elliptic phase, makes possible a direct first-order transition between the phases with linear and circular wave polarizations.

These phase diagrams complete the study of the homogeneous part of the model free energy. At the following step we refine the model to analyze its stability with respect to inhomogeneous fluctuations which are important in soft systems

with Goldstone degrees of freedom. The large-scale behavior of the Goldstone angles φ_1 and φ_2 are driven by the inhomogeneous terms in the free energy. Taking into account inhomogeneous terms, one finds eleven independent invariants appearing in the free energy density $F_{\text{tot}}(I_1 \dots I_{11})$:

$$\begin{aligned}
 I_1 &= \rho_1^2 + \rho_2^2, I_2 = \rho_1^2 \rho_2^2, \\
 I_3 &= \left(\frac{d\rho_1}{dz} \right)^2 + \rho_1^2 \left(\frac{d\varphi_1}{dz} \right)^2 + \left(\frac{d\rho_2}{dz} \right)^2 + \rho_2^2 \left(\frac{d\varphi_2}{dz} \right)^2, \\
 I_4 &= \rho_1^2 \left(\frac{d\varphi_1}{dz} \right) - \rho_2^2 \left(\frac{d\varphi_2}{dz} \right), \quad I_5 = \left[\rho_1^2 \left(\frac{d\varphi_1}{dz} \right) + \rho_2^2 \left(\frac{d\varphi_2}{dz} \right) \right]^2, \\
 I_6 &= \left\{ \left(\frac{d\rho_1}{dz} \right)^2 + \rho_1^2 \left(\frac{d\varphi_1}{dz} \right)^2 - \left(\frac{d\rho_2}{dz} \right)^2 + \rho_2^2 \left(\frac{d\varphi_2}{dz} \right)^2 \right\}^2 \\
 I_7 &= \left\{ \left(\frac{d\rho_1}{dz} \right)^2 + \rho_1^2 \left(\frac{d\varphi_1}{dz} \right)^2 - \left(\frac{d\rho_2}{dz} \right)^2 + \rho_2^2 \left(\frac{d\varphi_2}{dz} \right)^2 \right\} \\
 &\quad \times \left[\rho_1^2 \left(\frac{d\varphi_1}{dz} \right) + \rho_2^2 \left(\frac{d\varphi_2}{dz} \right) \right], \\
 I_8 &= (\rho_1^2 - \rho_2^2) \left[\rho_1^2 \left(\frac{d\varphi_1}{dz} \right) + \rho_2^2 \left(\frac{d\varphi_2}{dz} \right) \right], \\
 I_9 &= (\rho_1^2 - \rho_2^2) \left\{ \left(\frac{d\rho_1}{dz} \right)^2 + \rho_1^2 \left(\frac{d\varphi_1}{dz} \right)^2 - \left(\frac{d\rho_2}{dz} \right)^2 + \rho_2^2 \left(\frac{d\varphi_2}{dz} \right)^2 \right\}, \\
 I_{10} &= \rho_1 \rho_2 \frac{d\rho_1}{dz} \frac{d\rho_2}{dz}, \quad I_{11} = \rho_1^2 \left(\frac{d\rho_1}{dz} \right)^2 + \rho_2^2 \left(\frac{d\rho_2}{dz} \right)^2. \quad (8)
 \end{aligned}$$

The stable states are then obtained by a classical Euler-Lagrange procedure. The Lifshitz-type invariants I_4 and I_8 make unstable the states with homogeneous Goldstone phases φ_1 and φ_2 . According to Dzyaloshinskii [31] the most probable periodic and quasi-periodic modulated structures satisfy the conditions $\varphi_1 = q_1 z + \varphi_1^{(0)}$, $\varphi_2 = q_2 z + \varphi_2^{(0)}$, and $d\rho_1/dz = d\rho_2/dz = 0$. This yields four phases. (I) $\rho_1 = \rho_2 = 0$: isotropic liquid, (II) $\rho_1 = \rho_2$, $q_1 = q_2$: modulated *C* phase, (III) $\rho_1 = 0$, $q_2 \neq 0$ or $\rho_2 = 0$, $q_1 \neq 0$: modulated *R* phase, (IV) $\rho_1, \rho_2, q_1, q_2 \neq 0$: modulated EL phase.

Replacing φ_i by $\varphi_i = q_i z + \varphi_i^{(0)}$ in the definition of the polarization wave given by Eqs. (1)–(3) gives

$$\begin{aligned}
 \vec{P}(z) &= \{ \rho_1 \cos[(k + q_1)z + \varphi_1^0] + \rho_2 \cos[(k - q_2)z + \varphi_2^0] \} \vec{e}_x \\
 &\quad + \{ -\rho_1 \cos[(k + q_1)z + \varphi_1^0] + \rho_2 \cos[(k - q_2)z + \varphi_2^0] \} \vec{e}_y. \quad (9)
 \end{aligned}$$

No new phase is stabilized with respect to the homogeneous analysis but all the low-symmetry states are characterized by spatial modulations of the Goldstone angles ($q_1, q_2 \neq 0$). However, the *C* and *R* “modulated” phases remain commensurate because they are characterized by a single wave vector $k + q_1$. In contrast, in the EL phase the vector wave is characterized by two distinct wave vectors $k + q_1$ and $k - q_2$ [Eq.

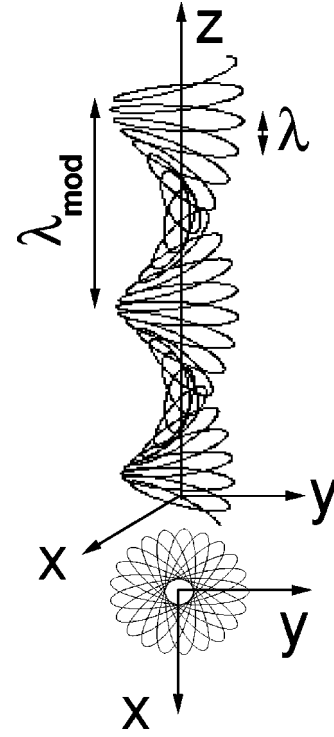


FIG. 4. Structure of the incommensurate elliptic phase with a period λ . Locally the structure is elliptic while the axes of the ellipse precess with a period λ_{mod} . The precession is evident on the projection of the structure onto the x - y plane. The projection has a flower-shape with a finite number of elliptic petals, because we have chosen for the picture a commensurate modulation wave vector. For general incommensurate structure the projection fills completely the disc surrounding the flower.

(9)], and the structure becomes actually incommensurate.

Let us finally describe the incommensurate elliptic structure. The wave vector k of the primary vector field is replaced with the temperature dependent term $K = k + (q_1 - q_2)/2$, whereas the modulation vector is $Q = (q_1 + q_2)/2$. The modulated vector wave appears then as the superposition of two perpendicular locally linear waves which reads (in the domain defined by $\varphi_1^{(0)} = \varphi_2^{(0)} = 0$):

$$\vec{P}(z) = 2(\rho_1 + \rho_2) \cos[Kz] \vec{e}_x(z) + 2(\rho_2 - \rho_1) \sin[Kz] \vec{e}_y(z), \quad (10)$$

where $\mathbf{e}_x(z) = \cos(Qz)\mathbf{e}_x - \sin(Qz)\mathbf{e}_y$ and $\mathbf{e}_y(z) = \sin(Qz)\mathbf{e}_x + \cos(Qz)\mathbf{e}_y$ are two perpendicular unit vectors turning within the $x+y$ plane with a wavelength $\lambda_{\text{mod}} = 1/Q$. $\mathbf{e}_x(z)$ and $\mathbf{e}_y(z)$ are parallel to the principal axes of the local projected ellipse. The incommensurate elliptic phase can be seen as a locally elliptic wave whose elliptic axes precess slowly along z . Let us stress that the ellipse turns without any deformation since the axes lengths $2|\rho_1 + \rho_2|$ and $2|\rho_1 - \rho_2|$ are independent of z . The corresponding structure is presented in Fig. 4.

The EL symmetries are broken by the incommensurate modulation except one twofold axis normal to the wave vector \mathbf{k} . The symmetry breakdown from orthorhombic to monoclinic is rather weak and the EL symmetry remains

locally close to the orthorhombic class. Thereby, the induced effects due to the monoclinic character of the elliptic phase are expected to be weak too.

III. SECONDARY PHYSICAL TENSORS

In this section we will consider the additional collective degrees of freedom of the medium which couple to the primary vector-wave order parameter $\mathbf{P}(z)$: (i) An axial vector wave $\mathbf{A}(z)$ which represents the spatial variations of the molecular plane orientation. (ii) A density wave which is induced in the rectilinear and elliptic phases and makes them smectic. (iii) Homogeneous tensors characterizing the macroscopic properties of these phases.

A. Polar and axial vector waves

The orientation of the molecule with respect to the layer normal is usually described in smectic phases by an axial vector \mathbf{A} normal to the tilt plane [32]. In bent-core systems the local orientation is described by the primary polar wave $\mathbf{P}(z)$ together with a transverse axial wave $\mathbf{A}(z)$ with the same wave vector \mathbf{k} . Since $\mathbf{P}(z)$ and $\mathbf{A}(z)$ span the same irreducible representation of the Euclidean symmetry group of the isotropic achiral liquid phase (or similarly of the nematic or smectic-*A* phases), $\mathbf{A}(z)$ is referred to as a ‘‘pseudoproper’’ [33] order parameter and has the same thermodynamic behavior as $\mathbf{P}(z)$. More precisely \mathbf{P} and \mathbf{A} are both pseudo proper order parameters so that consider \mathbf{P} as primary or \mathbf{A} as primary is theoretically arbitrary. Replacing \mathbf{P} with \mathbf{A} everywhere in Sec. I provides exactly the same theory with the same predictions. Which vector dominates and induces the other one at the microscopic level affects the values of the actual phenomenological coefficients but not the structure of the theory. In particular the pseudoproper feature means that if in a region of the theoretical phase diagram \mathbf{A} is strong and \mathbf{P} is weak at the first order isotropic-elliptic transition, then in a symmetric part of the phase diagram their roles will be reversed.

The general expression of $\mathbf{A}(z)$ is the same as that for $\mathbf{P}(z)$ given in Eq. (3), where the components $\eta_{1,2}$ have to be replaced with the complex amplitudes of \mathbf{A} : $\xi_1 = a_1 e^{i\psi_1}$ and $\xi_2 = a_2 e^{i\psi_2}$. The equilibrium values of ξ_1, ξ_2 are determined by their bilinear coupling with the primary order parameter $\eta_1 \xi_1^* - \eta_2 \xi_2^* + \eta_1^* \xi_1 - \eta_2^* \xi_2$. Minimization of the coupled free energy with respect to a_1, a_2, ψ_1 , and ψ_2 yields the following equilibrium values for $\mathbf{A}(z)$ and $\mathbf{P}(z)$.

The axial and polar waves are parallel in the circular phase

$$\vec{A}(z) = a_1 \begin{pmatrix} \cos(kz + \phi_1) \\ \sin(kz + \phi_1) \end{pmatrix}, \quad \vec{P}(z) = \rho_1 \begin{pmatrix} \cos(kz + \phi_1) \\ \sin(kz + \phi_1) \end{pmatrix} \quad (11a)$$

while they are perpendicular in the *R* phase:

$$\vec{A}(z) = 2a \sin\left(kz + \frac{\phi_1 - \phi_2}{2}\right) \begin{pmatrix} -\sin\left(\frac{\phi_1 + \phi_2}{2}\right) \\ -\cos\left(\frac{\phi_1 + \phi_2}{2}\right) \end{pmatrix},$$

$$\vec{P}(z) = 2\rho \cos\left(kz + \frac{\phi_1 - \phi_2}{2}\right) \begin{pmatrix} \cos\left(\frac{\phi_1 + \phi_2}{2}\right) \\ -\sin\left(\frac{\phi_1 + \phi_2}{2}\right) \end{pmatrix}. \quad (11b)$$

In *R* the maximums of one wave coincide with the zeroes of the second wave.

In the elliptic phase one has

$$\begin{aligned} \vec{A}(z) &= (a_1 - a_2) \cos\left(kz + \frac{\phi_1 - \phi_2}{2}\right) \begin{pmatrix} \cos\left(\frac{\phi_1 + \phi_2}{2}\right) \\ -\sin\left(\frac{\phi_1 + \phi_2}{2}\right) \end{pmatrix} \\ &\quad - (a_1 + a_2) \sin\left(kz + \frac{\phi_1 - \phi_2}{2}\right) \begin{pmatrix} \sin\left(\frac{\phi_1 + \phi_2}{2}\right) \\ \cos\left(\frac{\phi_1 + \phi_2}{2}\right) \end{pmatrix}, \\ \vec{P}(z) &= (\rho_1 + \rho_2) \cos\left(kz + \frac{\phi_1 - \phi_2}{2}\right) \begin{pmatrix} \cos\left(\frac{\phi_1 + \phi_2}{2}\right) \\ -\sin\left(\frac{\phi_1 + \phi_2}{2}\right) \end{pmatrix} \\ &\quad + (\rho_1 - \rho_2) \sin\left(kz + \frac{\phi_1 - \phi_2}{2}\right) \begin{pmatrix} \sin\left(\frac{\phi_1 + \phi_2}{2}\right) \\ \cos\left(\frac{\phi_1 + \phi_2}{2}\right) \end{pmatrix}. \end{aligned} \quad (11c)$$

\mathbf{A} and \mathbf{P} are not parallel except at special positions where the local symmetry increases up to C_2 . The projections of \mathbf{A} and \mathbf{P} onto the x - y plane give two ellipses with parallel axes. The corresponding great and small axis magnitudes are $|\rho_1 - \rho_2|$, $(\rho_1 + \rho_2)$ for \mathbf{P} and $|a_1 - a_2|$, $a_1 + a_2$ for \mathbf{A} . Comparing Eq. (11a)–(11c) with Figs. 1 and 2 yields the interpretation of $\mathbf{A}(z)$ as the tilt vector. Indeed, in *C*, \mathbf{P} and \mathbf{A} are parallel and the molecular plane is rotated around \mathbf{P} . In *R*, \mathbf{A} cancels at positions where \mathbf{P} is maximum so that in the antiferroelectric configuration the molecules are not tilted while in the anti-clinic configuration the molecules are tilted.

B. Scalar waves

In the vector-wave mechanism the density wave does not preexist the orientational ordering process leading to the phases *C*, *R*, and EL. So, one of the main unconventional features associated with this mechanism is the absence of smectic order in the *C* phase and the induced secondary character of the smecticity in the phases *R* and EL. Thus the smecticity of these structures is much less pronounced in these systems, at least close to the isotropic liquid phase, than in conventional smectic phases.

The periodicity of the induced density wave in *R* and EL is the half of the wavelength $\lambda = 2\pi/k$ because the symmetry

groups of all the ordered phases contain a twofold helical rotation axis. The corresponding density increment reads $\Delta\rho(z)=\delta\cos(2kz+\alpha)$. The corresponding coupled free energy reads

$$F_{\Delta/P}=F_P(\rho_1,\rho_2)+\frac{\alpha_\Delta}{2}\delta^2+\gamma_\Delta\delta\rho_1\rho_2\cos(\varphi_1-\varphi_2-\alpha). \quad (12)$$

Minimization of $F_{\Delta/P}$ with respect to δ and α yields the following behavior of δ and α .

(i) $\varphi_1-\varphi_2=\alpha$ for $\gamma_\Delta<0$ and $\varphi_1-\varphi_2=\alpha+\pi$ for $\gamma_\Delta>0$. In the first case the maximums of the density coincide with the maximums of \mathbf{P} and with the minimums of \mathbf{A} . In the second case the maximums of the density coincide with the minimums of \mathbf{P} and with the minimums of \mathbf{A} , leading to two physically different situations. Namely, the R phase appears in the first case as antiferroelectric and almost not tilted and in the second case as anticlinic with almost zero polarization.

(ii) $\delta\propto\rho_1\rho_2$. Thus, in the circular phase $\delta=0$ and no smectic modulation of the density occurs. In the phases R and EL, δ varies as $(T-T_R)$ in the R phase and $(T-T_{ELC})$ in the EL phase, in the vicinity of isotropic-rectilinear transition temperature T_R and of the $C\rightarrow$ EL transition temperature T_{ELC} , respectively. As the system approaches T_R or T_{ELC} the density modulation vanishes much faster than \mathbf{P} . Thus close to the transition temperatures the smectic character of R and EL is very weak.

Since the stability of thin films is closely related to their smecticity, we expect considerable difficulties in film preparation in the C phase and, close to the liquid state, in phases R and EL as well. Nevertheless the preparation can be made possible, even in the C phase, by the presence of walls between domains of opposite handedness or by the smecticity induced by the free surfaces of the films. Indeed a domain wall has an internal smectic structure. This property can be understood by considering the actual symmetry of the wall, which contains only the elements belonging simultaneously to the two domains, so that the continuous helical operations of a single domain are broken. Consequently the purely discrete translational symmetry remaining in the system gives a smectic structure to the wall.

Similar qualitative conclusions can be dressed about the x-ray diffraction behavior in the C phase. In the absence of domain walls and of surface induced smecticity, no diffraction peaks could be observed in usual x-ray experiment though resonant x-ray diffraction should display peaks at k and $-k$ corresponding to the single harmonic of the vector field in the C phase. However, in a realistic system containing smectic domain walls, usual x-ray diffraction patterns should show peaks at $\pm k, \pm 2k, \dots$. In the phases R and EL at sufficiently low temperature usual x-ray peaks should also be observed at $\pm k, \pm 2k, \dots$

C. Homogeneous tensors

The anisotropic part $\varepsilon_{ij}-Tr(\varepsilon)\delta_{ij}/3$ of the optic tensor ε is a traceless symmetric second-rank tensor [34]. It is uniaxial in C and biaxial in R and EL. In the biaxial phases

its eigenvectors are directed along x , y , and z . When one takes into account the incommensurability of the EL phase the preceding axes are slightly rotated about the y direction corresponding to the twofold symmetry axis of the structure. One part of this tensor, namely, $\varepsilon_{xx}+\varepsilon_{yy}$ is proportional to $\rho_1^2+\rho_2^2$ and varies close to T_C as $(T-T_C)$. Another part, expressing the planar optical biaxiality can be written as $\xi=\varepsilon_{xx}-\varepsilon_{yy}-2i\varepsilon_{xy}=|\xi|e^{i\beta}$. Its coupling with the order parameter gives the following contribution to the free energy: $|\xi|\rho_1\rho_2\cos(\varphi_1+\varphi_2-\beta)$ resulting in the relation $|\xi|\propto\rho_1\rho_2$. Hence $|\xi|$ vanishes as $(T-T_R)$ in the vicinity of the $R\rightarrow$ L transition temperature T_R .

Let us finally consider the third rank homogeneous tensor e_{ilk} (with symmetry $e_{ilk}=e_{ikl}$) which determines the electro-optic response of the mesophases and can be directly measured by second-harmonic generation experiments. In the R and C phases all the components e_{ilk} are cancelled. Locally in the elliptic phase with D_2 point group (commensurate approximation) the components, e_{xyz} , e_{yzx} , and e_{zxy} , of the tensor are nonzero.

On applying the electric field in EL along one of the twofold rotation axes, the symmetry reduces to the rotation parallel to the field. Accordingly the principal axes of the optic tensor, which are locked along the symmetric directions x, y, z in the zero-field phase, can rotate around the direction of the field. Applying \mathbf{E} along O_y induces a rotation of two principal axes to an angle $\delta_y=2e_{yxz}E/|\varepsilon_{zz}-\varepsilon_{xx}|$ with respect to the x and z directions, respectively. The rotation is clockwise for a given field polarity and counterclockwise for the opposite polarity. Along the same way for a given polarity the rotation sense in one domain is opposite to that in another domain of different chirality. If one applies the field along O_x the rotation angle is $\delta_x=2e_{xyz}E/|\varepsilon_{zz}-\varepsilon_{yy}|$. Since e_{xyz} and e_{yxz} are independent coefficients they can have different signs. Thus, the rotation can be clockwise as the field is applied along x and counterclockwise as it is applied along O_y . Applying the field normally to the wave vector (\mathbf{k}/O_z) in the incommensurate EL phase induces a rotation which varies along z . At positions where the long axis of the ellipse (i.e., one of the twofold axis of the underlying commensurate structure) is parallel to the field, the rotation angle is given by δ_x whereas it is given by δ_y at positions where the short axis (other twofold axis) is parallel to \mathbf{E} .

IV. RESPONSE TO EXTERNAL FIELDS

External fields such as the electric field or chiral doping deform the structures and break the symmetry groups of the ordered phases. These symmetry breakdowns yield modifications in the phase sequences. Several phases can merge into a single phase (elliptic and rectilinear for the chiral doping or circular and elliptic under electric field). Conversely several distinct phases can be created by the electric field from a single zero-field phase. This is the case for the elliptic and rectilinear phases, which lead to two and three phases, respectively.

A. Chiral doping

Concentration c of chiral molecules modifies the free energy of the system:

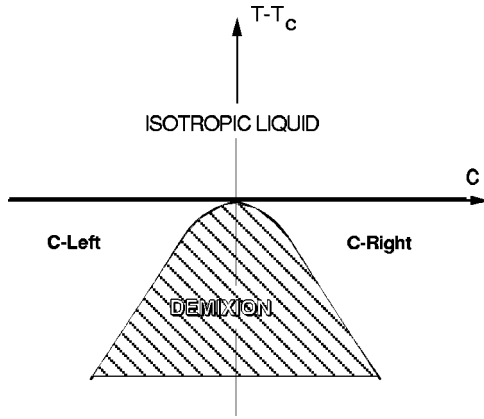


FIG. 5. Temperature (T) concentration of a chiral doping (c) phase diagram. At zero concentration the circular phase is stable. For nonzero concentrations the isotropic liquid (L) and the circular right-handed (for $c > 0$) and left-handed (for $c < 0$) phases are stabilized. Below the zero-concentration critical temperature T_c , the right and left circular phases can coexist. The corresponding demixion region is represented by the hatched area.

$$F_{c/P} = a_1(\rho_1^2 + \rho_2^2) + b_1 \rho_1^2 \rho_2^2 + \frac{a_2}{2}(\rho_1^2 + \rho_2^2)^2 + \frac{b_2}{2} \rho_1^4 \rho_2^4$$

$$d(\rho_1^2 + \rho_2^2)\rho_1^2 \rho_2^2 + v(\rho_1^2 - \rho_2^2)c + \frac{A}{2}c^2. \quad (13)$$

The main effects resulting from the coupling of \mathbf{P} with c are (i) the difference between the rectilinear and elliptic phases disappears, (ii) the transition temperature between the isotropic and circular phases increases, (iii) demixion between the domains of opposite chiralities in the circular phase takes place.

Minimization of $F_{c/P}$ provides the conditions of stability for the circular and elliptic phases. For $b_1 > 0$ the elliptic phase is not stable. The corresponding phase diagram in the (c, T) plane is indicated in Fig. 5. The right and left-handed circular domains are stabilized at low and high concentrations, respectively. The transition temperature between the isotropic liquid state and the circular phase increases linearly with the concentration in each domain, in such a way that the transition temperature is always higher than the transition temperature T_{c0} in the achiral compound. In the intermediate concentration range and below T_{c0} the phase diagram presents a zone of coexistence of the two domains. This zone of demixion is symmetric with respect to the axis $c=0$. Similar behavior can be foreseen in the elliptic phase.

B. Structures under applied electric field

Applying a weak electric field \mathbf{E} within the smectic $x-y$ plane first yields the orientation of the structure by the field. This effect does not take place in the circular phase which is macroscopically isotropic in the $x-y$ plane. In the R phase and in the approximately commensurate EL phase two situations should be distinguished.

(a) After the orientation \mathbf{E} is not parallel to one of the twofold C_2 rotation axes of the structure. The symmetry of R

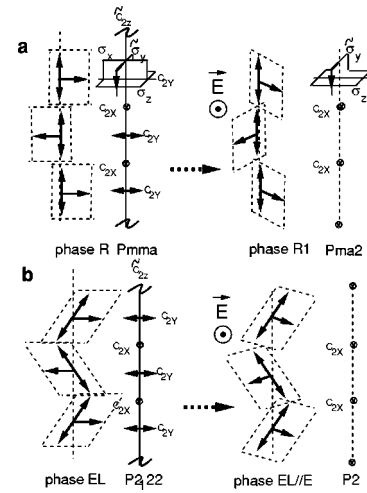


FIG. 6. Symmetries and molecular configurations corresponding to the flip process in the (a) zero-field R phase, (b) $R1$ phase, (c) zero-field EL phase, (d) $EL_{//}$ phase.

becomes monoclinic (space group Pm) and that of EL becomes triclinic (space group $P1$). Accordingly the macroscopic polarization \mathbf{P}_0 is not parallel to the applied field. We will denote R_E and EL_E these two low-symmetry phases induced by the field.

(b) One of the two C_2 rotation axes orients in the direction of the field. Since these axes are not equivalent, two different types of behavior are associated with the two possible final orientations. In the region of low fields, the local polarization at any position in the phase tends to orient along the direction of the field and the structure is distorted. The symmetry group of the resulting structure is given by the intersection of the undistorted phase symmetry group with that of the field. These two behaviors can be denoted as the flip and the flop processes, respectively. Let us first describe these processes in the R phase (Figs. 6 and 7).

Flip process. The plane of the polarization is initially normal to the direction of the field. For finite field values the polarizations of two adjacent layers rotate in opposite senses in order to get closer to the direction of \mathbf{E} . During this process the twofold rotation axis normal to the smectic layers (C_{2z}), the axis parallel to the initial polarization (C_{2y}) and the mirror plane normal to $\mathbf{E}(\sigma_z)$ are lost (Fig. 6(a)). The resulting symmetry of the distorted R phase (denoted $R1$) corresponds to the orthorhombic group $Pma2$. The axial vector \mathbf{A} is not modified by the field at the interfaces between the smectic layers. At the center of the layers a longitudinal component of \mathbf{A} appears. The local symmetry prevents a rotation of the molecular plane, which remains normal to the layers. The corresponding molecular configuration is presented in Fig. 6(a).

Flop process. The polarization remains everywhere parallel to \mathbf{E} . The polarization in one layer is in the direction of \mathbf{E} while the polarization in the adjacent layer is opposite to \mathbf{E} . For finite field the latter polarization decreases while the former increases. This breaks the twofold rotation axes (C_{2z} and C_{2x}) and the mirror plane (σ_y) normal to \mathbf{E} (Fig. 7(a)). The resulting orthorhombic symmetry group of the distorted structure (denoted $R2$) is $Pmm2$. The axial vector \mathbf{A} remains

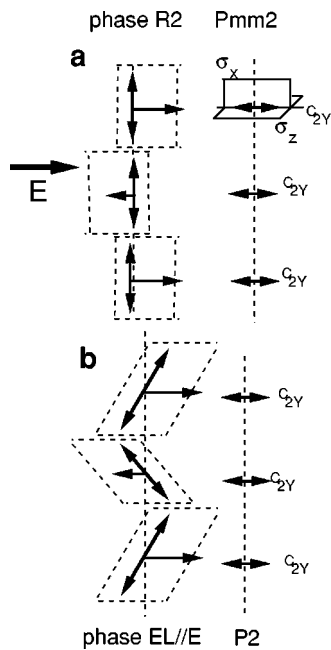


FIG. 7. Symmetries and molecular configurations corresponding to the flop process in (a) the $R2$ phase, (b) the $EL_{//}$ phase. In the $R2$ phase the polarization directions in two adjacent smectic layers are opposite and their magnitudes are different. The molecular planes are not tilted so that two adjacent layers have the same thickness. In the $EL_{//}$ phase the molecules are tilted. The tilt angle is different in two adjacent smectic layers, which consequently, have different thickness.

zero at the center of the layers so that the single effect of the field on the molecular configuration is to increase the disorder in the layer where \mathbf{P} is opposite to \mathbf{E} and to increase the order in the layers where \mathbf{P} and \mathbf{E} are parallel.

Thus the two processes yield two rectilinear phases $R1$ and $R2$ with different groups belonging to the same orthorhombic class. The corresponding molecular configurations are shown in Figs. 6(a) and 7(a).

In the (commensurate) elliptic phase the situation is more complex. In the flip process the field is normal to the local polarization \mathbf{P} at the center of the smectic layers, i.e., where \mathbf{P} is maximum. In the distorted phase this maximal polarization rotates toward the direction of the field, as in the R phase. However at positions where \mathbf{P} is minimum (at the interfaces between two adjacent layers), the polarization is parallel to the field and it is not rotated but either increased (where \mathbf{P} is in the same direction than \mathbf{E}) or decreased (where \mathbf{P} is in the opposite direction). Accordingly the process is, in fact, mixed: flip at the maximums and flop at the minimums of \mathbf{P} . At the center of the smectic layers this field induced state (denoted $EL_{//}$) differs from its rectilinear analog $R1$ by the presence of a nonvanishing transverse (in the x - y plane) axial vector indicating a tilt of the molecular plane with respect to the smectic planes. \mathbf{P} and \mathbf{A} are not parallel because the molecular polarization fluctuates asymmetrically with respect to the smectic layers in such a way that the mean polarization nevertheless remains parallel to the layers.

In the flop process the field is parallel to the local polarization at the center of the layers where \mathbf{P} is maximum. Thus,

the flop occurs at the maximums of the polarization while the flip occurs at positions where \mathbf{P} is minimum. At the center of the layers the axial vector remains parallel to \mathbf{P} but with different amplitudes in two adjacent layers. As in the $R2$ phase the only difference induced by the field is to increase the flip-flop disorder in the layer where \mathbf{P} is opposite to the field.

In both cases the symmetry of the distorted phase is described by the monoclinic group $P2$ containing a single two-fold axis. Unlike the situation in the R phase, the distinction between flip and flop in the elliptic phase is purely quantitative and, accordingly, the field produces a single elliptic parallel phase. The field does not affect the translational symmetries of the structures. However the breakdown of the screw twofold axis (C_{2z}) normal to the smectic layers and of the corresponding gliding plane (σ_y) leads to a doubling of the smectic lattice spacing in the phases $R2$ and EL_E (but not in $R1$ where σ_y is not broken). Indeed two adjacent layers become nonequivalent in the distorted structures and an additional Bragg peak at $q=k$ should be evidenced in usual (nonresonant) x-ray diffraction experiments. From the optical point of view the phases $R1$ and $R2$ keep the same property as without any field, i.e., the three eigenvectors of the optical tensor are not rotated by \mathbf{E} . In the $EL_{//}$ phase one eigenvector is not modified (parallel to the C_2 axis) whereas the two other vectors rotate around the twofold axis.

The action of the field on C makes this phase elliptic. The long axis can be either parallel or normal to the field direction [Fig. 6(b)], according to the sign of the coefficient coupling the order parameter with \mathbf{E} [γ in Eq. (14)].

In the incommensurate elliptic phase, the single twofold rotation axis turns towards a direction parallel to the field and the symmetry of the zero-field structure is not modified. In the vicinity of this axis the structure of the system is similar to that of the $EL_{//}$ phase described above. The corresponding free energy of interaction with the field is locally minimal. Far from the axis the structure is in the configuration (denoted EL_E) which does not correspond to a minimum of the interaction energy. The field tends to orient the local structure in the $EL_{//}$ configuration while the elastic energy of the incommensurate helix tends to maintain the initial structure. As a consequence the helix is globally distorted and unwound by the field. The field favors a multisolitons regime in which adjacent stripes, corresponding to the orientation of the long and short elliptic axes of the underlying commensurate structure are oriented along the field, are separated by thin walls. On increasing the field strength the size of the stripes corresponding to the orientation with the smallest interaction energy increases.

C. Phase diagrams

We have shown that under low applied fields the circular phase becomes elliptic whereas the rectilinear and elliptic phases are distorted in either parallel or nonparallel configurations (in the "parallel" phases the field is parallel to one of the twofold axes of the zero-field structure). At higher fields \mathbf{E} tends to increase the symmetry of the structure in order to make closer the symmetry group of the structure and that of

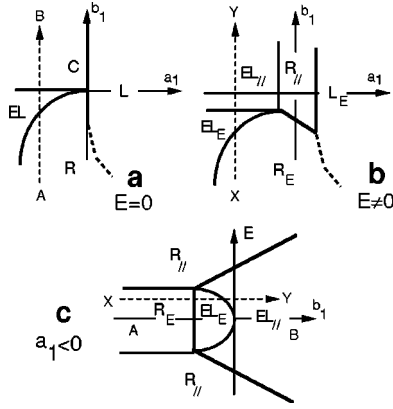


FIG. 8. (a) Zero-field minimal phase diagram. (b) Deformation of the minimal phase diagram under a low applied electric field E . (c) b_1 - E phase diagram with a_1 constant and negative. The thermodynamic paths (AB) and (XY) represented by thin dashed straight lines in (a) and (b) are indicated. $R_{//}$ represents either $R_1(\gamma > 0)$ or $R_2(\gamma < 0)$. Thick dashed curves and thick plain curves represent first-order and second-order transition lines, respectively.

the field itself. Thus the nonparallel configurations become parallel and the elliptic phase becomes rectilinear. At still higher fields the order may be completely destroyed and the system undergoes a transformation into the polarized liquid state (L_E). However, we will demonstrate that the opposite situation in which the field favors the ordered state can also take place. Close to the critical temperature of the transition at zero field the electric field can, in this case, transform the polarized liquid into the rectilinear phase.

The free energy describing the field behavior of the vector field model is given by

$$F_E = a_1(\rho_1^2 + \rho_2^2) + b_1\rho_1^2\rho_2^2 + \frac{a_2}{2}(\rho_1^2 + \rho_2^2)^2 + \frac{b_2}{2}\rho_1^4\rho_2^4 + \gamma P_0^2\rho_1\rho_2 \cos \Delta - P_0 E \cos \alpha + \frac{1}{2\kappa}P_0^2, \quad (14)$$

where α is the angle between \mathbf{P}_0 and \mathbf{E} . $\Delta = \varphi_1 + \varphi_2 - 2\omega$ where ω is the angle between \mathbf{P}_0 and Ox . Minimization of F yields six stable phases

(1) The polarized liquid phase $T \times C_{\infty v}$: $\rho_1 = \rho_2 = 0$, $\mathbf{P}_0 = \kappa \mathbf{E}$,

(2) the R_1 phase (flip) $Pma2$: $\rho_1 = \rho_2$, $\alpha = 0$, $\Delta = \pi$,

(3) the R_2 phase (flop) $Pmm2$: $\rho_1 = \rho_2$, $\alpha = 0$, $\Delta = 0$,

(4) the R_E phase Pm : $\rho_1 = \rho_2$,

(5) The $EL_{//}$ phase $P2$: $\alpha = 0$, $\Delta = 0$ or π ,

(6) The EL_E phase $P1$: general case.

A number of theoretical temperature-field phase diagrams is associated with the free energy F_E . We will first present those corresponding to the “minimal” zero-field phase diagram (Fig. 8) in which all the transitions are second order and the direct elliptic \rightarrow isotropic transformation is impossible (except at the isolated four-phase point). We will describe then the more realistic situation in which this transformation is possible across a first-order transition line. The latter case is associated with the Landau expansion of the

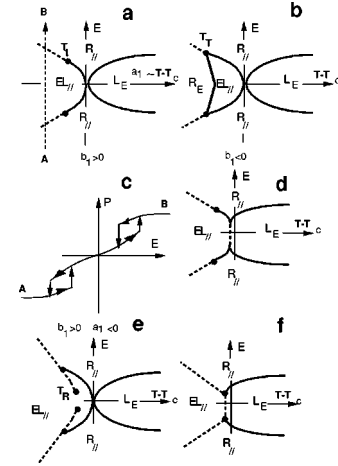


FIG. 9. Temperature (T) field (E) phase diagrams resulting from the minimal zero-field diagram represented in Fig. 8(a), for b_1 constant and a_1 varying linearly with T . (a) $b_1 > 0$. The zero-field phase stable below T_c is circular. It becomes elliptic parallel when the field is switched on and rectilinear parallel above a second-order transition line. The line becomes a first-order transition line at temperatures below the tricritical point T_T . Above T_c the polarized liquid state is stable at low fields. Above a critical field the liquid state undergoes a field-induced transition toward the rectilinear parallel ($R_{//} = R_1$ or R_2) phase. (b) $b_1 < 0$. The stable zero-field phases are E and R . They transform into the $R_{//}$ phase above a critical field. The three ordered structures merge at the triple point T_T . (c) Hysteresis curve (polarization P vs field E) along the thermodynamic path AB indicated by a dashed line in (a). (d)–(f) Modification of the phase diagram (a) resulting from higher degree coupling terms. The direct elliptic \rightarrow liquid first-order transition becomes possible (d). An isostructural transition within the elliptic stability domain separates the almost circular from the almost rectilinear elliptic states (e). The corresponding first-order transition line ends at the critical point (T_R).

free energy taking into account higher degree terms [than those in Eq. (14)].

(i) The low-field deformation of the minimal phase diagram is presented in Fig. 8(b). At low fields the circular phase becomes elliptic parallel to the field ($EL_{//}$) while the EL phase remains elliptic but non parallel (EL_E). Similarly the R phase remains rectilinear but nonparallel (R_E). A parallel R phase is stabilized between the liquid and the $EL_{//}$ phase. Thus the direct transformation from the EL phase into the isotropic liquid across a four-phase point becomes impossible under the applied field. Figure 8(c) displays the phase diagram in the b_1 -field plane. At high fields both R and EL become parallel to the field (R_1 or R_2 according to the sign of the coefficient γ). At still higher fields the elliptic phase becomes rectilinear. R is the single stable phase at high fields.

Figure 9 displays temperature-field phase diagrams for fixed b_1 . For $b_1 > 0$ [Fig. 9(a)] the circular phase is stable at zero field below T_c . High fields stabilize the R phase below as well as above T_c . This remarkable behavior means that above T_c the achiral liquid state can become unstable under a sufficiently strong applied field which makes it polar smectic. The field-induced ordering can be second order and the

corresponding critical field varies as $(T - T_c)^{1/2}$. Below T_c the circular phase is stable at zero field and it becomes elliptic when the field is switched on. At higher fields it undergoes a second-order phase transition into the R phase. The corresponding transition line becomes first-order at a tricritical point (T_t). The hysteresis curve associated with this transition is represented in Fig. 9(c). For $b_1 < 0$ [Fig. 9(b)] the phases R and EL are stable below T_c at zero field. The liquid, the phases R and EL transform into the parallel R phases at high fields. The stability domains of the phases $R_{//}$, $EL_{//}$, and R_E merge at a triple point (T_T).

Taking into account higher degree coupling terms in the free energy modifies the previous phase diagram as represented in Figs. 9(d)–9(f). A first-order transition between the liquid state and the elliptic phase becomes possible [Fig. 9(d)]. A first-order isostructural transition can also occur inside the elliptic stability domain [Fig. 9(e)]. Below the corresponding critical field the elliptic phase has an almost circular structure, while it is almost rectilinear above the transition. The transition line has a terminal critical point (T_R).

(ii) Let us now consider the deformation by the field of the nonminimal phase diagram in which a first-order isotropic \rightarrow elliptic transition line is present. The zero-field phase diagram is presented in Fig. 10(a). Close to the elliptic domain the transitions $C \rightarrow$ liquid and $R \rightarrow$ liquid become first order.

Let us consider the thermodynamic path indicated in the zero-field phase diagram [Fig. 10(a)]. Along this path the system is rectilinear at low temperature, elliptic within an intermediate range and isotropic at high temperature. Applying E and varying T along this path yields the phase diagrams presented in Figs. 10(b)–10(d). The $R_{//}$ phase, which was stable at high fields in Fig. 8, becomes metastable and is no more present in the phase diagram. Thus, below T_c the stable high-fields phase is liquid. The $R_{//} \rightarrow EL_{//}$, $R_{//} \rightarrow L_E$ and $EL_{//} \rightarrow L_E$ transition temperatures decrease with the field.

Along the two zero-field thermodynamic paths crossing in Fig. 10(a) the second-order $L \rightarrow C$ and $L \rightarrow R$ transition lines, respectively, the metastability of the high-fields $R_{//}$ phase can also take place. In the case when the R -phase is stable at zero field the transition to the liquid state may be either first or second order [Fig. 11(a)]. In the case when the circular phase is stable at zero field the parallel rectilinear phase is stabilized within an intermediate field range [Fig. 11(b)]. The temperature stability interval of this R phase may be limited by a triple point T_R [Fig. 11(c)].

V. DISCUSSION

The bent-core mesophases condense directly from the isotropic liquid, usually without any intermediate smectic-A or nematic phase. Only few exceptional cases of smectic A or nematic can be found in the experimental literature [35–37]. These classical mesophases are stabilized in systems of particular molecules with a large opening angle ψ which behave almost as calamitic mesogens. This rule is supported by numerical simulations [22] which state that the Sm-A phase can exist only for $\psi > 165^\circ$, the antiferroelectric (AFE) phases be-

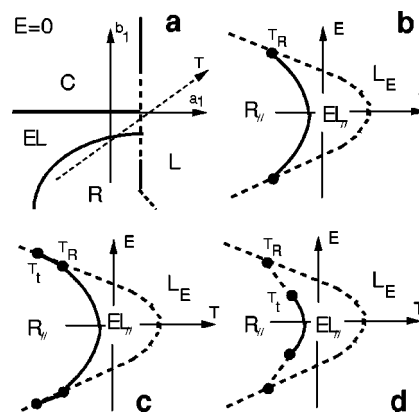


FIG. 10. Temperature-field phase diagrams resulting from the deformation of the nonminimal zero-field diagram (a). According to the degree of non-linearity and to the signs of the phenomenological coefficients in the free energy, various topologies may be predicted including various triple (T_T) and tricritical (T) points.

ing unstable within this range. For $\psi > 135^\circ$ the nematic phase can coexist with AFE structures. However, almost all the bent-core mesogens exhibiting the unconventional AFE phases correspond to an opening angle $\psi < 135^\circ$. A surface stabilized smectic A phase has also recently been evidenced in thin films [38] for molecules with $\psi > 140^\circ$. Along the same line transitions from Sm-A or Sm-C to B_2 have been observed in binary systems formed with bent-core mixed with calamitic mesogens [39]. A “demixion” is observed between the classical phases (Sm-A, Sm-C and nematic) which are stabilized at low bent-core concentration and phase B_2 which is stable at high concentration.

Two different textures of the bent-core phase denoted B_2 are observed in bulk samples: “racemic” and “homochiral.” In a structural model proposed by Link *et al.* [2] these two textures are associated with two distinct phases, denoted racemic and homochiral model phases. The structure of the homochiral model phase coincides with the elliptic phase. It is confirmed by a whole series of experiments. By contrast,

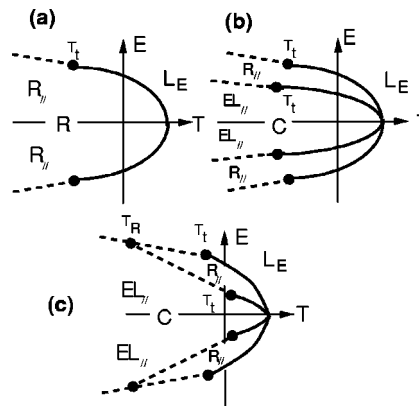


FIG. 11. Temperature-field phase diagrams where the coupling coefficients favor the liquid state. In contrast to the case of the diagrams shown in Fig. 9, the liquid state remains stable at high fields. The field destabilizes the ordered states, which undergo phase transformations toward the liquid phase above critical fields. The corresponding transition lines may be first or second order.

we think that the organization of the racemic texture remains an open question. In our approach the only achiral structure is the R phase which seems at first view a good candidate for describing the racemic texture. However, the interpretation of two systematically coexisting textures over the full stability temperature range of phase B_2 as distinct phases (racemic and homochiral model phases, on the one hand, or EL and R on the other) is impossible from the point of view of thermodynamics. We propose for this reason to identify the homochiral texture with single domains of EL and the racemic texture with several small domains of EL with opposite chiralities.

Recently an untilted antiferroelectric smectic phase has been disclosed in banana systems by Eremin *et al.* [21] (denoted C_P in Ref. [11] or Sm- AP_A in Ref. [22]). This achiral phase exhibits the molecular structure predicted for the R phase. It is optically biaxial and shows an AFE switching current behavior. The AFE chiral B_7 phase appears just below the liquid state. It differs from phase B_2 by its extraordinary textures, its weak smectic character in the temperature region close to the isotropic liquid and its 2D large-scale modulations [10]. We propose its possible identification with the circular phase.

A. Other theories

Structural models of polar smectic layers composed by bent-core molecules have been considered by Brand *et al.* [40]. The one-layer structures are obtained by intersecting the symmetry group of the Sm-A layers with that of a bent-core molecule. Different orientations of the molecule with respect to the symmetry axes of the layer give rise to different point groups and, consequently, to different structures. The highest possible symmetry C_{2v} yields a polar layer in which the molecular plane is not tilted. When the polarization reverses in two successive layers the structure (C_{PA}) is antiferroelectric (this structure coincides with our R phase). For an orientation with C_2 symmetry the structure becomes chiral and gives rise to an antiferroelectric structure coinciding with the elliptic phase. Similarly, C_S and C_1 groups lead to achiral antiferroelectric phases (C_{B_2}, C_{B_1}) and several chiral phases. However, this work is limited to the enumeration of the structures only. Their stability is not investigated and only low-field effects are described.

Kats *et al.* [41] have considered a semimicroscopic model in which three tensors break the rotational and achiral symmetry of the Sm-A phase: One axial and one polar vectors along with a pseudoscalar. In order to keep locally an in-plane two fold axis they impose to the two vectors to be parallel. Four phases can then be stabilized in which two tensors condense with the same periodicity as the smectic lattice while the third tensor remains homogeneous. This model yields four phases: Two achiral phases (one antiferroelectric and synclinic and the other ferroelectric and anticlinic) and two chiral phases (one synclinic ferroelectric and one anticlinic and antiferroelectric). The latter one coincides with our elliptic phase. The symmetries, structures, and physical properties of these phases are not worked out in this model.

A thermodynamic model based on the same ideas has been proposed by Roy *et al.* [42]. Starting from the parent Sm-A it predicts five *ferroelectric* phases after condensation of two independent order parameters: One axial and one polar homogeneous vectors. In order to fit their theory with the antiferroelectric character of bent-core systems, the authors invoke a helical winding of the polarization due to a flexoelectric term in the inhomogeneous free energy. In this continuous approach the modulation of the polarization is long range and cannot give rise to an antiferroelectric phase but rather to a Sm- C^* -type structure characterized by an helical pitch much larger than the layers thickness. Even by assuming a giant flexoelectric coefficient, the temperature-dependent pitch has no reason in this theory to lock to a value corresponding to two smectic layers.

Selinger [43] has proposed an Ising-type model investigating the “antichiral” phases occurring in racemic mixtures of chiral bent-core molecules. Starting from a smectic phase he considers a pseudoscalar wave with the smectic periodicity. He can thus investigate the action of chiral doping on the antichiral to homogeneously chiral phase transition. This approach uses a scalar order parameter which cannot (purposely) explain the apparition in the Sm-A of the polar and axial orders. They are assumed to preexist in each layer, unlike our model, in which the condensation of the antiferroelectric states are fully 3D effects since the layers formation is a consequence of the process.

The previous approaches assume a parent Sm-A phase which is usually not observed in pure bent-core systems. Thus, the stabilization of the predicted phases can result only from a coupled instability involving in the liquid state at least three order parameters: The smectic density wave together with the polar and axial homogeneous vectors. Such situation is thermodynamically extremely unlikely. Moreover this mechanism would necessarily stabilize some phases corresponding to the condensation of only one or two order parameters (Sm-A, Sm-C, polar liquid, ...). Indeed, one can assume that in a few compounds the thermodynamic coefficients take very specific values yielding the simultaneous onset of three independent order parameters, however the realization of these conditions in all the studied molecular series is, for us, unbelievable.

To summarize, these approaches (i) do not explain the stability of the two-layer antiferroelectric phases (except Ref. [41]), (ii) assume a Sm-A parent structure which is not observed in most cases, and (iii) imply several unlikely simultaneous instabilities. On the contrary vector-wave theory predicts antiferroelectric phases, one of them with the structure of the homochiral B_2 phase, which are stabilized directly from the liquid state. Moreover, as in unconventional superconductors, this very simple mechanism involves a single order parameter accounting for the complex properties of its ordered phases. One can notice that our approach holds also if one starts from a nematic phase (because all the low symmetry groups are subgroups of the nematic group) and needs only a few adaptations (e.g., the C phase becomes elliptic) if one starts from a Sm-A phase. Accordingly it can also describe the transitions occurring in binary mixtures from the nematic and Sm-A calamitic phases [39].

B. Structure of phase B_2 .

The molecular arrangement in phase B_2 has been determined by electro-optic measurements in bulk samples and thin films. Since the case of the homochiral texture is not controversial we will only discuss in this section three hypothesis (racemic model, R phase, and multidomain of EL) concerning the racemic texture. With an opening angle ψ about $100^\circ - 140^\circ$ the bent-core molecules are optically biaxial. The two corresponding optic axes are normal to the molecular polarization [2]. Since the molecules have C_{2v} symmetry group, the two axes are tilted symmetrically with respect to the molecular plane. This property permits to optically distinguish the R phase, the EL phase, and the racemic model phase. In the R phase the optic tensor is identical in two adjacent layers. Moreover the two optic axes of the layer are tilted symmetrically with respect to the layer normal. In the racemic model two adjacent layers are also optically indistinguishable, but the two optic axes are now tilted to different angles with respect to the layer normal. The same behavior occurs in the elliptic phase, however, in two adjacent layers the directions of the two optic axes are rotated to π .

In thin freely suspended films, within the temperature region of stability of the bulk B_2 phase, Link *et al.* observed a biaxial antiferroelectric achiral structure. The main optical characteristics of this structure are (i) the tilt of an optic axis with respect to the layer normal, (ii) the coexistence under an electric field of two domains with their optic axes rotated to π . Assuming the identification of the racemic texture with the R phase, the observed tilt of an optic axis could be explained by the intrinsic biaxiality of the layers discussed above. For further conclusions the determination of the directions of the two optic axes is necessary. In thin films of the R phase under low electric fields four domains can coexist (two series of two optically indistinguishable domains). This fact is in qualitative agreement with the observed domain structure in films. However, the two domains are not necessarily rotated to an angle π in R (in fact, neither in the racemic model since in films under electric field it presents the same domain pattern as R).

In bulk samples the homochiral state is usually observed inside circular domains with the smectic layers normal to the substrate. In such a domain, the extinction cross observed with polarized light rotates under electric field in opposite directions after field reversal [2,44,45]. In a circular domain formed within the EL phase, the wave vector \mathbf{k} is radial and the twofold rotation axes of the elliptic phase are normal and parallel to the plane of the domain [Fig. 12(a)] respectively. These twofold axes indicate the directions of the principal axes of the optic tensor at each point in the domain. At zero field this configuration leads to an extinction cross parallel to the polarizer and analyzer directions [Fig. 12(b)]. When the field is applied normally to the domain, the twofold axis C_{2y} is not modified while the two other symmetry axes are dropped out, yielding a rotation of the principal axes of the tensor together with that of the extinction cross [Fig. 12(c)]. We have shown in Sec. III C that the field-induced rotation of the optic tensor ε is given by the law $\varepsilon_{xz} = e_{yxz} E_y$ where the third-rank tensor component e_{yxz} has nonzero value in the

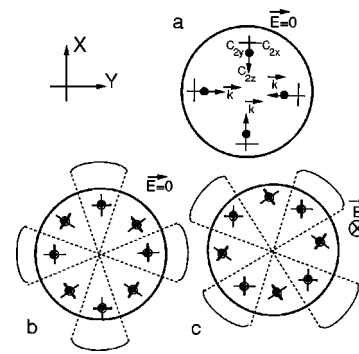


FIG. 12. Field-induced rotation of the extinction cross in a circular domain of the elliptic phase. (a) The smectic layers are normal to the plane of the figure and the wave vector \mathbf{k} is radial. The local twofold symmetry axes are either normal to \mathbf{k} (C_{2x} and C_{2y}) or parallel (C_{2z}). (b) Orientation of the principal axes of the optic tensor at various positions inside the circular domain. The axes are parallel to C_{2x} , C_{2y} , and \mathbf{k} . The extinction cross observed under polarized light with a polarizer parallel to X and an analyzer parallel to Y is indicated by dashed lines. (c) The application of an electric field \mathbf{E} normal to the plane of the figure breaks the twofold axes C_{2x} and C_{2z} . The optic axes within the plane (x, \mathbf{k}) of the figure are no more locked and rotate in a sense which depends on the polarity of the field. The extinction cross rotates to the same angle.

elliptic phase. As the field changes its polarity (E_y becomes negative) ε_{xz} changes its sign and the optic tensor axis rotates in the opposite direction. In contrast, in the R phase $e_{yxz} = 0$ and no rotation should be observed. Indeed, under applied electric field the R phase has the point symmetry C_{2v} that locks the principal axes of the optic tensor and forbids any rotation. This absence of rotation is observed in the racemic regions, which are thus compatible with the R phase properties.

However, it is more reasonable to look for another interpretation of the racemic regions in terms of specific textures occurring in the elliptic phase. At the $L \rightarrow$ EL transition many small domains with opposite handedness must be created in order to restore at the macroscopic level the broken achiral symmetry of the liquid phase. The resulting texture appears achiral at large scale. Under special conditions, e.g., under the influence of the surface or close to structural defects, the size of the monodomains can be increased. This happens, for instance, in the circular domains discussed above. The multidomain texture behaves thus as the racemic regions while the monodomains of the elliptic phase shows the behavior of the homochiral regions. In the racemic regions the absence of rotation of the extinction cross is thus explained by the fact that the right-handed domains rotate clockwise whereas the left-handed domains rotate counterclockwise. In this approach the chiral character of the individual domains is dropped out while the tilt of the macroscopic optic axis persists since the domain walls keep the biaxial symmetry.

In conclusion, we think that available experimental data permit us to make a clear-cut conclusion about the elliptic structure of the homochiral texture but that the question remains open for the racemic texture. In any case, the systematic coexistence in the bulk of two distinct phases over a large temperature interval cannot be taken as a basis for the data interpretation.

C. Properties of phase B_2

Second harmonic generation experiments show that the single nonzero component of the SHG tensor is very small in phase B_2 [46,47]. The only symmetry classes which combine chirality and zero SHG tensor are 422, 622, $\infty 2$, and 432 [48]. Since $\infty 2$ is the point group of the C phase, the small SHG signal can be interpreted as a strong circular character of the elliptic phase at zero field. On increasing the electric field the signal varies smoothly up to a critical field where it sharply increases and exhibits a strong hysteresis. In the high-field region the SHG tensor shows C_2 symmetry. In the elliptic model, the high-fields phases $R1$ or $R2$ have the symmetry C_{2v} , which is ruled out by the previous experimental results. However, the elliptic phase has C_2 symmetry under low fields and can undergo a first-order isostructural transition [see Fig. 9(e)] from a low-field almost circular configuration toward a high-field strongly elliptic (or possibly almost rectilinear) configuration. The corresponding hysteresis is in agreement with the experimental data.

The chirality of the banana phases has been probed by chiral doping experiments [49]. It is observed that the domains with one chirality are favored by the doping concentration. In a chemically heterogeneous system this leads to a demixion of the regions with opposite chirality. The sample becomes homogeneous with uniform chirality only for high doping concentrations. These results coincide with the theoretical prediction of the vector-wave model indicating the demixion of the left- and right-handed domains at low concentrations and single handedness at high concentrations (see Fig. 5).

Another important feature of our model has been experimentally verified [50]. Sufficiently high electric fields applied in the isotropic phase above the critical temperature induces the formation of textures characteristic of the elliptic phase. Thus, our prediction of a field-induced instability of the isotropic phase is confirmed.

The broad stripes evidenced in the homochiral regions under applied fields have been interpreted as chiral domains with optic axes rotating in opposite directions depending on the handedness of the domain [45,51,52]. This effect can also be due to the incommensurate superstructure of the elliptic phase. Indeed, we have claimed in Sec. III that under applied fields the helical superstructure can transform into a periodic pattern of domains. In two adjacent domains the handedness is the same but with the short and long elliptic axes, respectively, parallel to the field. Applying the field parallel to the long and short axes (coinciding with the twofold axes parallel to the smectic layers of the commensurate EL phase) can result in opposite optical rotations if the coefficients e_{yxz} and e_{xyz} have different signs (see Sec. III C). Thus the apparent chirality difference in adjacent domains can be in fact due to different signs of e_{yxz} and e_{xyz} in a single chiral domain striped by solitonic walls.

Thin stripes are also observed in the racemic texture under an electric field, and they disappear above a threshold voltage [52]. Within our model the R phase becomes nonparallel R_E at low fields and parallel R_1 or R_2 at higher fields. In the nonparallel state two orientational domains, rotated to an angle π about the field axis, are stabilized. Above the

critical field the system undergoes a second-order transition toward the parallel R phase which possesses a single domain under fields. Thus the R phase hypothesis is in agreement with these observed properties of the racemic texture.

D. The C_P phase

The existence of an untilted rectilinear phase in our model is made possible by the fact that though the primary polarization wave induces an axial (tilt) wave, the molecules can be polarized and untilted at the centers of the layers when the phase shift between these two waves is $\pi/2$. The recent discovery by Eremin *et al.* [21] of such an achiral antiferroelectric structure in compounds of molecules with an opening angle $\psi=106^\circ$ confirms the possibility of an achiral AFE state in banana systems. This phase was denoted C_P (or C_{PA}), following a nomenclature introduced by Brand *et al.* [40,53]. It exhibits the characteristic double-loop AFE hysteresis curve with very high saturation polarization. In contrast to the homochiral B_2 phase (EL) no optical switching is observed as the polarity of the applied electric field is reversed. In the structural model proposed by Eremin *et al.*, the symmetry of the layers is C_{2v} . Since the polarization alternates in adjacent layers, the space group belongs to the orthorhombic D_{2h} class. All these features are in a perfect agreement with the structure of the R phase proposed by the vector-wave model.

E. The B_7 phase

The chiral B_7 phase is usually observed just below the liquid state [9]. It is characterized by its extraordinary textures such as spiral, double spirals, oval, and circular domains and stripes which are usually interpreted as resulting from a helical structure. Its dimensionality remains controversial and both 1D and 2D structures have been proposed. Recent measurements have shown a large-scale modulation of the 1D structure along a direction perpendicular to the layer normal [10]. Neglecting at the microscopic scale this modulation and assuming the one-dimensional character for phase B_7 , we are going now to discuss the identification of phase B_7 with the circular phase.

At the isotropic $\rightarrow B_7$ transition no jump in the physical properties, such as the saturation polarization, has been evidenced in agreement with the possibility of a second order or weakly first order isotropic $\rightarrow C$ transition. The main problem of the proposed identification comes from the nonsmectic character of the bulk C phase while the B_7 phase is currently assumed to exhibit a low symmetry smectic structure. Observation of sharp x-ray peaks and formation of stable fibers [54] seem to confirm the smectic character of phase B_7 . However, since on the one hand fibers were also evidenced in bent-core nematics [54] they do not permit us to firmly conclude that phase B_7 is intrinsically smectic. On the other hand the x-ray diffraction patterns obtained on cooling from the liquid state indicate a single very wide peak down to 5 K below the isotropic $\rightarrow B_7$ transition [10]. Along the

same way, thin films of phase B_7 are very difficult to stabilize. We interpret these two preceding properties as the effects of a weak (induced) smecticity in the B_7 phase at high temperature. Indeed a slight distortion of the circular phase makes it elliptic and consequently smectic. This distortion can be produced by the film surfaces or, similarly, by the interfaces between two domains of opposite chiralities. A high density of such surfaces is optically observed in the textures of the B_7 and B_2 phases. This assumption is supported by fracture microscopy image [10] showing randomly dispersed small regions in phase B_7 which can explain the

apparent symmetry lowering in phase B_7 while this phase is often observed between the high symmetry liquid and the B_2 phases.

We can then propose the following tentative scenario: In the high temperature region of the B_7 phase the structure is described by the circular wave with weak induced smectic order. This phase can be stabilized within a temperature interval close to the isotropic liquid. For lower temperatures the system undergoes a transformation into a more ordered (maybe elliptic) smectic structure with a 2D modulation in the direction of the layers.

-
- [1] T. Niori, T. Sekine, J. Watanabe, T. Furukawa, and H. Takezoe, *J. Mater. Chem.* **6**, 1231 (1996).
- [2] D. R. Link, G. Natale, R. Shao, J. E. Maclennan, N. A. Clark, E. Korblova, and D. M. Walba, *Nature (London)* **278**, 1924 (1998); G. Heppke, A. Jakli, D. Kroerke, C. Lohning, D. Lotzsch, S. paus, S. Rauch, and K. Sarma (Unpublished); W. Weissflog, C. Lischka, I. Benné, T. Scharf, G. Pelzl, S. Diele, H. Kruth, and I. Wirth, *Ferroelectrics* **212**, 169 (1998); R. Macdonald, F. Kentischer, P. Warnick, and G. Heppke, *Phys. Rev. Lett.* **81**, 4408 (1998).
- [3] A. Fukuda *et al.*, *J. Mater. Chem.* **4**, 997 (1994); I. Musevic, R. Blinc, and B. Zeks, *The Physics of Ferroelectric and Antiferroelectric Liquid Crystals* (World Scientific, Singapore, 2000).
- [4] G. Pelzl, S. Diele, and W. Weissflog, *Adv. Mater. (Weinheim, Ger.)* **11**, 707 (1999).
- [5] W. Weissflog, C. Lischka, I. Benné, T. Scharf, G. Pelzl, S. Diele, and H. Kruth, *Proc. SPIE* **14**, 3319 (1998).
- [6] S. Diele, S. Grande, H. Kruth, and C. Lischka, *Ferroelectrics* **212**, 169 (1998).
- [7] T. Sekine, T. Niori, M. Sone, J. Watanabe, S. W. Choi, Y. Takanishi, and H. Takezoe, *Jpn. J. Appl. Phys., Part 1* **36**, 6455 (1997).
- [8] J. Watanabe, T. Niori, T. Sekine, and H. Takezoe, *Jpn. J. Appl. Phys., Part 2* **37**, L139 (1998).
- [9] G. Pelzl, S. Diele, A. Jäkli, C. Lischka, G. Pelzl, I. Wirth, and W. Weissflog, *Liq. Cryst.* **26**, 135 (1999).
- [10] N. A. Clark *et al.*, 19th International LCC, Edinburgh, 2002 (unpublished); International FLCC, Dublin, 2003 (unpublished).
- [11] T. Sekine, Y. Takanishi, T. Niori, J. Watanabe, and H. Takezoe, *Jpn. J. Appl. Phys., Part 2* **36**, L1201 (1997).
- [12] G. Heppke, and D. Moro, *Science* **279**, 1872 (1998).
- [13] R. Balian and N. R. Werthamer, *Phys. Rev.* **131**, 1553 (1963); P. W. Anderson, and P. Morel, *Phys. Rev. Lett.* **5**, 136 (1960).
- [14] K. Ueda and T. M. Rice, *Phys. Rev. B* **31**, 7114 (1985).
- [15] M. Sigrist and K. Ueda, *Rev. Mod. Phys.* **63**, 239 (1991).
- [16] A. J. Leggett, *Rev. Mod. Phys.* **47**, 331 (1975); L. P. Pitaevskii, *Sov. Phys. JETP* **37**, 1267 (1960).
- [17] L. Landau, E. M. Lifshitz, and L. P. Pitaevskii, *Statistical Physics* (Pergamon Press, Oxford, 1980), Pt. 2, Sec. 54; D. Mermin, *Phys. Rev. A* **9**, 868 (1973).
- [18] V. Lorman and B. Mettout, *Phys. Rev. Lett.* **82**, 940 (1999).
- [19] Yu. M. Gufan, G. M. Vereshkov, P. Tolédano, B. Mettout, V. Lorman, and R. Bouzerar, *Phys. Rev. B* **51**, 9219 (1995).
- [20] E. I. Kats, *Sov. Phys. Usp.* **27**, 42 (1984).
- [21] A. Eremin, S. Diele, G. Pelzl, H. Nadasi, W. Weissflog, J. Salfetnikova, and H. Kresse, *Phys. Rev. E* **64**, 051707 (2001).
- [22] Y. Lansac, P. K. Maiti, N. A. Clark, and M. A. Glaser, *Phys. Rev. E* **67**, 011703 (2003).
- [23] *Ferroelectric Liquid Crystals* edited by J. W. Goodby (Gordon and Breach, Philadelphia, 1991).
- [24] L. D. Landau and E. M. Lifshitz, *Statistical Physics* (Pergamon, London, 1958).
- [25] P. G. deGennes and J. Prost, *The Physics of Liquid Crystals* (Clarendon Press, Oxford, 1993).
- [26] In the full thermodynamic potential, all the branches of the star of \mathbf{k} appear and the free energy is an integral of the right-hand side of Eq. (7a)–(7c) over the continuous star. When a single branch is active all the terms cancel in the integral except those associated with the active branch and F reduces to Eq. (7a)–(7c).
- [27] Yu. M. Gufan, *Sov. Phys. Solid State* **13**, 175 (1971); *Structural Phase Transitions* (Nauka, Moscow, 1982); J. C. Tolédano and P. Tolédano, *The Landau Theory of Phase Transitions* (World Scientific, Singapore, 1987).
- [28] C. J. Bradley and A. P. Cracknell, *The Mathematical Theory of Symmetry in Solids* (Clarendon Press, Oxford, 1972).
- [29] Y. Galerne and L. Liebert, *Phys. Rev. Lett.* **64**, 906 (1990).
- [30] E. I. Kut'in, V. L. Lorman, and S. V. Pavlov, *Sov. Phys. Usp.* **34**, 497 (1991).
- [31] I. E. Dzyaloshinskii, *Sov. Phys. JETP* **19**, 960 (1964).
- [32] M. Pikin, *Structural Transformations in Liquid Crystals* (Gordon and Breach Science Publishing, 1990); V. L. Lorman, *Mol. Cryst. Liq. Cryst. Sci. Technol., Sect. A* **262**, 437 (1995).
- [33] Yu. A. Izyumov and V. N. Syromiatnikov, *Phase Transitions and Crystal Symmetries* (Nauka, Moscow, 1984).
- [34] L. D. Landau and E. M. Lifshitz, *Quantum Mechanics* (Pergamon, London, 1958).
- [35] I. Wirth *et al.*, *J. Mater. Chem.* **11**, 1642 (2001).
- [36] D. Shen, S. Diele, G. Pelzl, I. Wirth, and C. Tschierske, *J. Mater. Chem.* **9**, 661 (2001).
- [37] S. Stojadinovic, A. Adorjan, S. Sprunt, H. Sawade, and A. Jakli, *Phys. Rev. E* **66**, 060701 (2002); P. J. Camp, *Can. J. Phys.* **111**, 9871 (1999).
- [38] D. A. Olson, X. F. Han, A. Cady, W. Weissflog, and C. C. Huang, *Phys. Rev. Lett.* **88**, 085504 (2002).
- [39] M. W. Schroder, S. Diele, G. pelzl, N. Pacenko, and W. Weiss-

- flog, *Liq. Cryst.* **29**, 1039 (2002).
- [40] H. R. Brand, P. E. Cladis, and H. Pleiner, *Eur. Phys. J. B* **6**, 347 (1998).
- [41] E. I. Kats and J. Lajzerowicz, e-print cond-mat/9912486.
- [42] A. Roy, N. V. Madhusudana, P. Tolédano, and A. M. Figueiredo Neto, *Phys. Rev. Lett.* **82**, 1466 (1999).
- [43] J. V. Selinger, *Phys. Rev. Lett.* **90** 165501 (2003).
- [44] J. P. Bedel, J. C. Rouillon, J. P. Marcerou, M. Laguerre, M. F. Achard, and H. T. Nguyen, *Liq. Cryst.* 103 (2000); J. P. Bedel, Ph.D. thesis, Bordeaux I, 2000.
- [45] G. Pelzl, S. Diele, S. Grande, A. Jakli, C. Lischka, H. Kresse, H. Schamllfuss, I. Wirth, and W. Weissflog, *Liq. Cryst.* **26**, 401 (1999).
- [46] R. Macdonald, F. Kentischer, P. Warnick, and G. Heppke, *Phys. Rev. Lett.* **81**, 4408 (1998).
- [47] J. Ortega, N. Pereda, C. L. Folcia, J. Extebarria, and M. B. Ross, *Phys. Rev. E* **63**, 011702 (2000); S. W. Choi, Y. Kinoshita, B. Park, H. Takezoe, T. Niori, and J. Watanabe, *Jpn. J. Appl. Phys., Part 1* **37**, 3408 (1998).
- [48] Yu. I. Sirotnin and M. P. Shaskolskaya, *Basics of Crystallography* (Nauka, Moscow, 1979).
- [49] J. Thysayutka, H. Niwano, H. Takezoe, and J. Watanabe, *J. Mater. Chem.* **11**, 2717 (2001).
- [50] V. Bourny, V. Lorman, J. Pavel, B. Mettout, and H. T. Nguyen, *Ferroelectrics* **276**, 127 (2001)
- [51] A. Jakli, S. Rauch, D. Löttsch, and G. Heppke, *Phys. Rev. E* **57**, 6737 (1998).
- [52] G. Heppke, A. Jakli, S. Rauch, and H. Sawade, *Phys. Rev. E* **60**, 5575 (1999).
- [53] H. R. Brand, P. E. Cladis, and H. Pleiner, *Macromolecules* **25**, 7223 (1992).
- [54] A. Jakli, D. Krierke, and G. G. Nair, *Phys. Rev. E* **67**, 051702 (2003).